Research Article

Nano Biomed Eng

NIR-IIb-emitted Er-coordination Polymer for Logic Gates and Optical Anticounterfeiting

Yanling Yang[1], Fengyue Wang[1], Shan Zhang[1], Hongxin Zhang[2], Zhen Yang[1]

[1] Strait Institute of Flexible Electronics (SIFE, Future Technologies), Fujian Key Laboratory of Flexible Electronics, Fujian Normal University and Strait Laboratory of Flexible Electronics (SLoFE), Fuzhou 350117, China

[2] Laboratory of Advanced Materials, Fudan University, Shanghai 200438, China

Corresponding author. E-mail: ifezhyang@fjnu.edu.cn

Received: Oct. 24, 2024; **Revised:** Nov. 8, 2024; **Accepted:** Nov. 22, 2024

Citation: Y.L. Yang, F.Y. Wang, S. Zhang, et al. Nir-iib-emitted er-coordination polymer for logic gates and optical anticounterfeiting. *Nano Biomedicine and Engineering*, 2025, 17(1): 143−150.

http://doi.org/10.26599/NBE.2024.9290107

Abstract

The second near-infrared window in a 1 500–1 700 nm region (known as the NIR-IIb region) presents low autofluorescence and a deep penetration depth, enabling a potential technology for effective imaging and anticounterfeiting applications. However, existing NIR-IIb-emitted fluorescence materials remain limited and possess low luminescent properties. In implementing the enhanced ~1 525 nm emission of the Er (III) complex in a nonorganic solvent, an amphiphilic diblock copolymer (PEG_{112}–PAA_{12}) was initially synthesized to coordinate with Er (III), and then certain Yb (III) was doped to form the PEG–PAA–Er/Yb complex. The complex shows a dramatic fluorescent enhancement of ~250-fold at ~1 525 nm in D_2O than that in H_2O under 980-nm laser irradiation, which is ascribed to the following factors: (1) The substitution of H_2O by D_2O can suppress the quenching effect of H_2O at ~1 470 nm to achieve the emission of PEG–PAA–Er; (2) the doping of Yb (III) enables the co-luminescence effect to PEG–PAA–Er to improve NIR-IIb emission. Notably, the PEG–PAA–Er/Yb complex can construct molecular logic gates with logic functions and optical anticounterfeiting by using the abovementioned fluorescence changes.

Keywords: NIR-IIb emission; PEG–PAA–Er; Yb; D_2O; optical anticounterfeiting

Introduction

The second near-infrared window (NIR-II, 1 000–1 700 nm), which has deep-tissue penetration and high spatial resolution, shows great superiority for bioimaging [1–10] and information storage and decoding [11, 12]. In particular, the NIR-IIb region (1 500–1 700 nm), which has lower autofluorescence and deeper penetration depth than the general NIR-IIa region (1 100–1 400 nm) [13], has attracted considerable attention. However, the extensive application of NIR-IIb fluorescence emission is limited because of the low number of optional probes and low emission capacity in the NIR-IIb region. Thus, developing novel NIR-IIb fluorescent probes and exploring their applications are necessary.

At present, NIR-IIb-emitted fluorescence probes are focused on quantum dots [14, 15], Er-based downconversion nanoparticles [16, 17], and Er complexes [18]. Among them, Er complexes, which are equipped with small-molecule properties and functional modification, gradually emerged as a popular NIR-IIb-emitted fluorescence probe. However, Er (III) is susceptible to vibrational

quenching by *X*–H (*X* is C, N, and O) oscillators from the surrounding coordination environment [19, 20]. Given the strong absorption of water molecules at ~1 470 nm, an Er (III)-based complex shows a significant spectral overlap around ~1 525 nm and energy transfer with H_2O, thereby limiting the fabrication of NIR-IIb-emitting Er-based probes. Although different strategies have been applied to enhance the NIR-IIb emission of the Er complex, such as the use of fluorinated ligands [21, 22], the formation of metallacrowns [23, 24], and NIR absorption ligands with high sensitization efficiency [18], the application of Er-based complexes with highly intensive NIR-IIb emission is still impeded.

In this study, an amphiphilic diblock copolymer (PEG_{112}–PAA_{12}) was synthesized through three steps, and a PEG–PAA–Er complex was prepared by using the coordination effect between the carboxyl group of PEG_{112}–PAA_{12} and Er (III). Moreover, a PEG–PAA–Er/Yb complex with ~1 525 nm emission is formed by doping Yb (III) into the prepared PEG–PAA–Er in D_2O, which is due to the combinational effect of the co-luminescence of Yb and low vibrations of D_2O (Scheme 1). This significant change in fluorescence signal promotes the construction of molecular logic gates and optical anticounterfeiting applications. This work provides a strategy for improving the NIR-IIb emission of the Er (III) complex at ~1 525 nm.

Experimental

Materials

Methoxypolyethylene glycol was purchased from Aladdin. D_2O, triethylamine (TEA), 2-bromoisobutyryl bromide, pentamethyldiethylenetriamine (PMDTA), dry dichloromethane (CH_2Cl_2), N,N-dimethylformamide (DMF), and tetrahydrofuran (THF) were purchased from Energy Chemical. Diethyl ether was purchased from Hushi. 4-Dimethylaminopyridine (DMAP) was purchased from Aladdin. Tert-butyl acrylate, trifluoroacetic acid (TFA), and cuprous bromide (CuBr) were purchased from Macklin. $ErCl_3$ and $YbCl_3$ were purchased from Beijing Hwrkchemical Co., Ltd. All chemicals were purchased and used as received without further purification unless otherwise stated. A dialysis bag was purchased from Sigma-Aldrich.

Instrumentation

Nuclear magnetic resonance (NMR) spectra were obtained using a Bruker AV-400 spectrometer. The chemical shifts were referenced to the residual solvent peaks and given in ppm. Transmission electron microscopic images were recorded by using a JEM 2100F microscope (Japan) operated at 200 kV. Ultraviolet (UV)–visible (Vis)–near infrared (NIR)

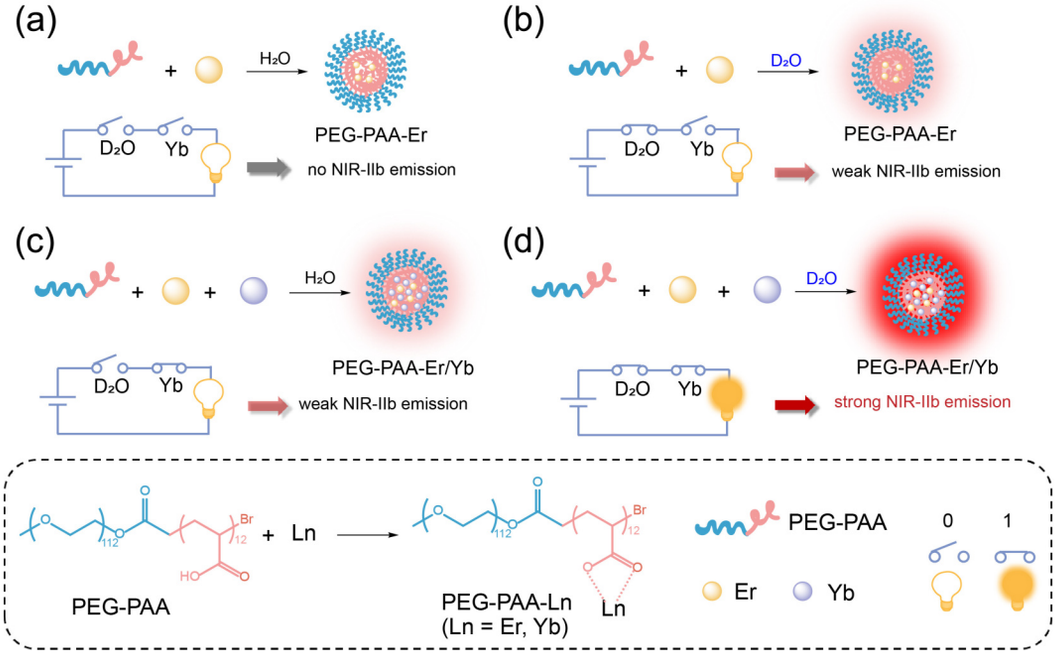

Scheme 1 Preparation, NIR-IIb emission mechanism, and anticounterfeiting of the PEG–PAA–Er complex in **(a)** H_2O and **(b)** D_2O and of the PEG–PAA–Er/Yb complex in **(c)** H_2O and **(d)** D_2O.

absorption spectra were collected by using a Lamda750S PerkinElmer at a scan rate of 2 000 nm/min. NIR-II fluorescence spectra were acquired by using the Edinburgh FLS980 fluorescence spectrometer. Quartz cuvettes (1 cm) were used to measure absorbance and emission. NIR-II fluorescence images were taken using the InGaAs camera (C-RED2, First Light Imaging Corp., France).

Synthesis and preparation

Synthesis of PEG_{112}–Br

A solution containing methoxypolyethylene glycol (200 mg, 1.0 eq), 2-bromoisobutyryl bromide (18 mg, 2.0 eq), TEA (9 mg, 2.2 eq), and DMAP (0.5 mg, 0.1 eq) dissolved in CH_2Cl_2 (15 mL) was stirred overnight under N_2 atmosphere. The reaction mixture was extracted using H_2O and dried using anhydrous Na_2SO_4. After filtration, the mixture was precipitated by adding ethyl ether to obtain PEG_{112}–Br.

Synthesis of PEG_{112}–TBA_{12}

A solution containing 100 mg of PEG_{112}–Br (1.0 eq), 8.5 mg of CuBr (3.0 eq), 256.3 mg of tert-butyl acrylate (100 eq), and 10 mg of PMDTA (3.0 eq) dissolved in dry DMF (15 mL) was stirred at 70 °C overnight under N_2 atmosphere. After reaction, the reaction mixture was exposed to the atmosphere under an ice bath to stop polymerization, and then THF was added to dilute the solution. The mixture was purified by Al_2O_3 flash column chromatography and evaporated. The residue was precipitated by adding ethyl ether and dried to obtain PEG_{112}–TBA_{12}.

Synthesis of PEG_{112}–PAA_{12}

PEG_{112}–TBA_{12} was (20 mg) dissolved in 1 mL of dry CH_2Cl_2 under N_2 atmosphere, and TFA (1 mL) was added dropwise to the abovementioned solution. After stirring overnight, the mixture was precipitated by adding ethyl ether to obtain PEG_{112}–PAA_{12}.

Preparation of PEG–PAA–Er in H_2O

A solution containing $ErCl_3$ (18.9 mg) dissolved in 0.5 mL of H_2O was slowly added to 0.5 mL of PEG_{112}–PAA_{12} (7.4 mg), and the reaction mixture was stirred for 24 h in 1.0 mL of MilliQ water at room temperature. Then, these samples were purified three times using a dialysis bag.

Preparation of PEG–PAA–Er/Yb in H_2O

A solution containing $ErCl_3$ (18.9 mg) dissolved in 0.5 mL of H_2O was slowly added to 0.5 mL of PEG_{112}–PAA_{12} (7.4 mg), and the reaction mixture was stirred for 24 h at room temperature to form PEG–PAA–Er. Different amounts of $YbCl_3$ were added to the PEG–PAA–Er aqueous solution, in which n_{Er}:n_{Yb} = 0.04, 0.1, 0.2, 0.4, 0.6. Then, the obtained PEG–PAA–Er/Yb_x (where x denotes the different doping amounts of Yb) was purified three times using a dialysis bag.

Preparation of PEG–PAA–Er in D_2O

First, 1.0 mL of D_2O solution was mixed with a PEG_{112}–PAA_{12} polymer (7.4 mg) and $ErCl_3$ (18.9 mg) and stirred at room temperature for 24 h. Then, the obtained samples were purified three times using a dialysis bag.

Preparation of PEG–PAA–Er/Yb in D_2O

First, 1.0 mL of D_2O was mixed with PEG_{112}–PAA_{12} polymer (7.4 mg) and $ErCl_3$ (18.9 mg) and stirred at room temperature for 24 h to form PEG–PAA–Er. Different amounts of $YbCl_3$ were added to the D_2O solution of PEG–PAA–Er, in which n_{Er}:n_{Yb} = 0.04, 0.1, 0.2, 0.4, and 0.6. Then, the obtained PEG–PAA–Er/Yb_x (x denotes the different doping amounts of Yb) was purified three times using a dialysis bag.

Results and Discussion

First, an amphiphilic diblock copolymer (PEG_{112}–PAA_{12}) was synthesized through three steps (Fig. S1 in the Electronic Supplementary Material (ESM)), which was characterized by ^{1}H NMR (Figs. S2–S4 in the ESM). Using PEG_{112}–PAA_{12}, the PEG–PAA–Er complex in H_2O was prepared via one-step reaction and characterized by using transmission electron microscopy (TEM, Fig. S5 in the ESM). The optical properties of the PEG–PAA–Er complex demonstrated the maximum absorption and emission wavelengths of DMSO at of 980 and ~1 525 nm, respectively (Figs. S6 and S7 in the ESM). The fluorescence intensity of ~1 525 nm gradually increased with the increase of Er (III) concentration, and the emission of PEG–PAA–Er was higher at ~1 525 nm under 980-nm laser irradiation than that under 808-nm laser (Fig. S7 in the ESM). This difference in emission might be due to the higher molar extinction coefficient of PEG–PAA–Er at 980 nm than that at 808 nm. However, PEG–PAA–Er

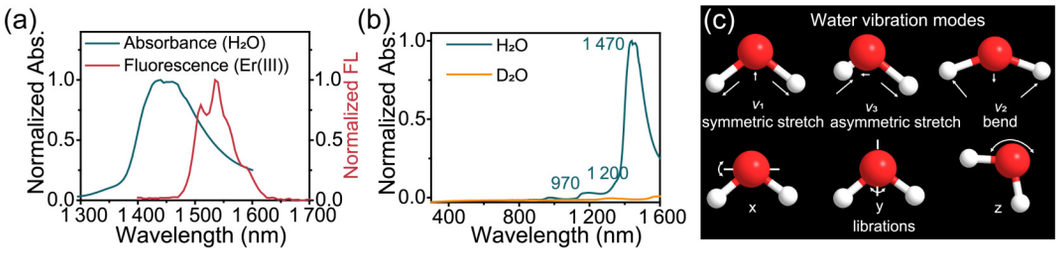

(d) Assignment of the IR vibrational absorption spectrum of liquid water

Wavelength (nm)	cm⁻¹	Assignment
1 470	6 800	$av_1 + bv_3$; a + b = 2
1 200	8 330	$av_1 + v_2 + bv_3$; a + b = 2
970	10 310	$av_1 + bv_3$; a + b = 3

(e) Main vibrations of liquid and dinary water

Vibration (s)	liquid H_2O (25 °C)		liquid D_2O (25 °C)	
	ν, cm⁻¹	ε_λ, M⁻¹ cm⁻¹	ν, cm⁻¹	ε_λ, M⁻¹ cm⁻¹
v_2	1 643.5	21.65	1 209.4	17.10
combination of v_2 +libration	2 127.5	3.46	1 555.0	1.88
v_1, v_3, and overtone of v_2	3 404.0	100.61	2 504.0	69.68

Fig. 1 (a) Normalized absorbance of H_2O and the fluorescence spectrum of the PEG–PAA–Er complex. **(b)** Normalized absorbance of H_2O and D_2O. **(c)** Schematic diagram of the vibrational mode of water molecules. **(d)** Assignment of the IR vibrational absorbance spectrum of liquid water. **(e)** Main vibrations of liquid H_2O and D_2O.

showed no NIR-IIb emission in H_2O. Thus, the absorbance spectrum of H_2O and the fluorescence spectrum of PEG–PAA–Er in DMSO were compared to achieve the NIR-IIb emission of PEG–PAA–Er in a nonorganic solution (Fig. 1(a)). The result showed an evident spectral overlap between the absorbance of H_2O and the emission of PEG–PAA–Er, as well as energy loss caused by the vibration of the hydroxyl group [25], thereby quenching the NIR-IIb emission of PEG–PAA–Er in H_2O. Moreover, H_2O featured the main absorption bands at ~970, ~1 200, and ~1 470 nm because of the contributions of symmetric stretch, asymmetric stretch, and bending of H_2O molecules (Figs. 1(b)–1(d)). Compared with H_2O, D_2O displayed a negligible absorbance in the wavelength range of 800–1 600 nm, which was ascribed to its lower molar extinction coefficient (Figs. 1(b) and 1(e)).

In investigating the effects on the NIR-IIb emission of PEG–PAA–Er from H_2O and D_2O, the PEG–PAA–Er complex was prepared in D_2O instead of H_2O and was characterized by TEM (Fig. S8 in the ESM). First, the fluorescence intensity of the PEG–PAA–Er and $ErCl_3$ solutions was compared under 808 and 980-nm excitation, respectively. The results indicated that the fluorescence intensity of the PEG–PAA–Er solution was higher than that of the $ErCl_3$ solution under the same conditions (Figs. 2(a) and 2(b)). Therefore, the PEG–PAA polymer can coordinate with Er (III), which increases the characteristic emission of Er (III). Simultaneously, the fluorescence emission of PEG–PAA–Er in D_2O was superior to that in H_2O, which enhanced by 2.50- and 5.39-fold under 808- and 980-nm excitation, respectively (Fig. 2(c)). Given the co-luminescence effect [26] of lanthanide complexes, different amounts of Yb (III) were doped into PEG–PAA–Er to prepare PEG–PAA–Er/Yb complexes in D_2O and H_2O to further improve the NIR-IIb emission of PEG–PAA–Er, which was characterized by TEM (Figs. S9 in the ESM and Fig. 2(d)). The prepared PEG–PAA–Er/Yb in D_2O possessed a pear-like morphology. PEG–PAA–Er±Yb displayed evident absorption at 980 nm in H_2O and D_2O (Fig. 2(e)). In H_2O, PEG–PAA–Er/Yb showed a negligible fluorescence intensity with the increase of Yb concentration under 808- and 980-nm laser irradiation (Figs. S10(a) and S10(c) in the ESM). In D_2O, PEG–PAA–Er/Yb showed a prominent fluorescence emission (Figs. S10(b) and S10(d) in the ESM), and the strongest fluorescence intensity was observed when the molar ratio of Er (III) and Yb (III) reached 0.04 under 980-nm laser irradiation. It was mainly because that the introduction of Yb (III) resulted in co-luminescence effect and –COOH of PEG–PPA coordinated with Er (III) changed the coordination environment of Er (III).

The fluorescence intensity of PEG–PAA–Er/Yb at ~1 525 nm in D_2O enhanced by 250- and 128-fold under 980- and 808-nm laser irradiation, respectively, compared with PEG–PAA–Er in H_2O (Figs. 2(f) and S11 in the ESM). These results indicated the absence of an enhancement effect during Yb (III) doping or when D_2O was used for PEG–PAA–Er (Figs. 2(a)–2(c)). On the contrary, a dramatic fluorescence enhancement was observed at ~ 1 525 nm during the doping of certain Yb (III) simultaneous with the substitution of H_2O by D_2O (Fig. 2(f)). This finding

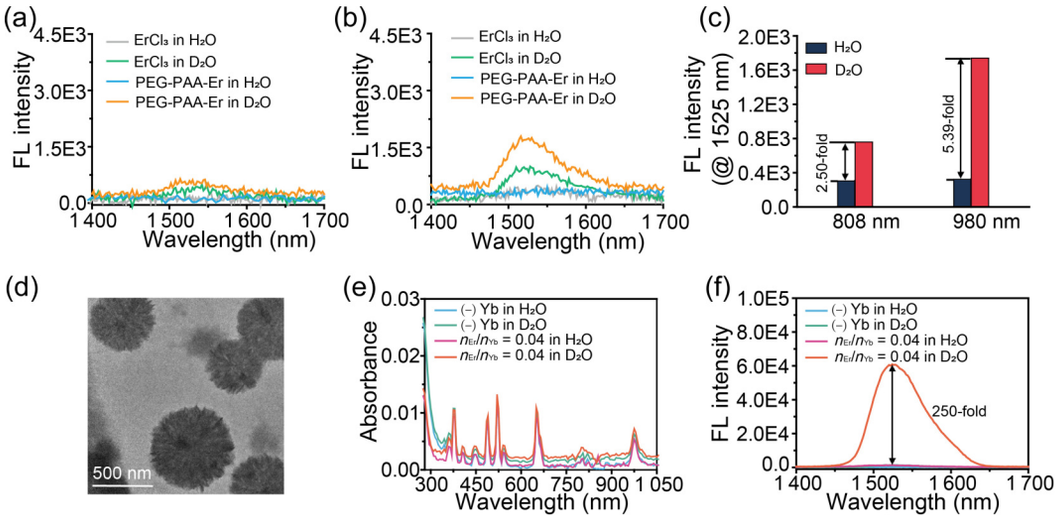

Fig. 2 NIR-IIb fluorescence emission of PEG–PAA–Er and $ErCl_3$ in H_2O and D_2O under **(a)** 808 nm and **(b)** 980 nm excitation, respectively. **(c)** NIR-IIb emission intensity of PEG–PAA–Er in H_2O and D_2O at 1 525 nm. **(d)** TEM of PEG–PAA–Er/Yb in D_2O. **(e)** Absorbance spectra of PEG–PAA–Er under the indicated conditions. **(f)** NIR-IIb emission spectra of PEG–PAA–Er under the indicated conditions under 980 nm excitation.

indicated that the combinational effect of doping Yb (III) and using D_2O could achieve fluorescence enhancement at ~1 525 nm. In addition, apart from the co-luminescence effect of lanthanide complexes, the introduction of small-molecule ligand could replace H_2O and participate in coordination with lanthanide ions, which can increase the emission of lanthanide complexes [27]. Therefore, we doped different amounts of Gd (III) and 1.10-phenanthroline (phen) into PEG–PAA–Er in D_2O to regulate NIR-IIb emission at ~1 525 nm (Fig. S12 in the ESM). However, PEG–PAA–Er showed no NIR-IIb emission under 980-nm laser excitation. These results indicated that PEG–PAA–Er could efficiently emit NIR-IIb fluorescence concurrently in D_2O and with Yb doping because of the induced energy loss and sensitization from Yb (III) to Er (III) [24]. However, PEG–PAA–Er cannot achieve *in vitro* and *in vivo* applications because the presence of water can remarkably influence NIR-IIb fluorescence emission in biological systems.

Optical anticounterfeiting and encryption have always been a matter of concern and exploration. Among the evident optical anticounterfeiting and encryption materials, lanthanide-based nanomaterials showcase diverse radiation absorption and emission because of their unique electronic layer structure, which are beneficial for use in diverse optical output anticounterfeiting. Therefore, lanthanide-based nanomaterials have been gradually applied for anticounterfeiting and encryption [28–34]. In particular, near-infrared fluorescent signals that are difficult to observe through the naked eyes dramatically improve the security of anticounterfeiting and encryption. Therefore, fluorescence emission at ~1 525 nm during Yb doping simultaneous with the presence of D_2O indicated the potential application of PEG–PAA–Er/Yb in information storage and anticounterfeiting. Furthermore, the efficient NIR-IIb emission of PEG–PAA–Er was used in the presence of D_2O and Yb to construct molecular logic gates, in which the chemical-encoded information as input has been converted to fluorescent signals as output, thereby resulting in information storage devices at the molecular level.

Thus, depending on the two input signals (D_2O and Yb), logic gates with AND logic functions were constructed. As shown in Figs. 2(f) and 3(a), no fluorescence emission at 1 525 nm was observed in the absence of both inputs; thus, the output became “0” (entry 1). In the presence of D_2O or Yb as input 1 and input 2, respectively, the weak fluorescence emission at 1 525 nm was not observed; thus, both outputs became “0” (entry 2 and entry 3). However, in the presence of both inputs, a strong fluorescence band at 1 525 nm was observed, and the output became “1”. Accordingly, the truth table value for the output forms an AND logic gate (Fig. 3(b)).

Given the AND logic gate application from the efficient NIR-IIb emission of PEG–PAA–Er through D_2O and Yb, the changes in NIR-IIb fluorescence

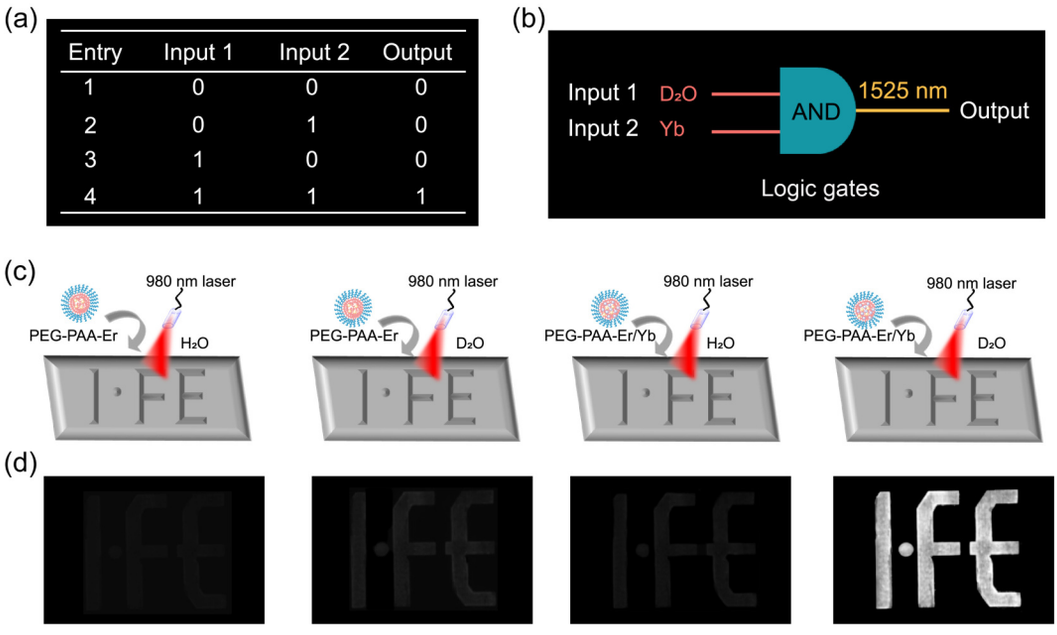

Fig. 3 (a) Truth table of logic gates. **(b)** Logic gate system using D_2O and Yb as inputs and the NIR-IIb emission intensity of PEG–PAA–Er at 1 525 nm as the output. **(c)** Experimental scheme of the information storage performance of PEG–PAA–Er. "I•FE" pattern drawn on the nonfluorescent mold using a writing brush dipped in fluorescent ink with PEG–PAA–Er in H_2O, PEG–PAA–Er in D_2O, PEG–PAA–Er/Yb in H_2O, and PEG–PAA–Er/Yb in D_2O. **(d)** Corresponding NIR-IIb fluorescence images of the "I•FE" handwriting using fluorescent solution under 980-nm laser illumination (Ex: 980 nm, 1 000 nm long-pass filter).

signal are sufficient for optical anticounterfeiting. NIR-IIb fluorescence images were designed on the basis of PEG–PAA–Er. In addition, PEG–PAA–Er or PEG–PAA–Er/Yb coordination polymers dispersed in H_2O and D_2O were used as the fluorescent ink. As depicted in Figs. 3(c) and 3(d), a writing brush dipped in fluorescent ink was used to draw patterns on a nonfluorescent mold. PEG–PAA–Er in H_2O was nonfluorescent under 980-nm laser irradiation. Furthermore, "I•FE" showed weak fluorescence signals in the presence of PEG–PAA–Er in D_2O or PEG–PAA–Er/Yb in H_2O. For PEG–PAA–Er/Yb in the D_2O-treated group, a strong "I•FE" fluorescence signal was observed. This observation indicated the potential application of Er-based coordination polymers in anticounterfeiting.

Conclusions

In this study, a PEG–PAA–Er coordination polymer was successfully prepared, and PEG–PAA–Er achieved NIR-IIb emission in nonorganic solutions by doping Yb and replacing H_2O with D_2O. The NIR-IIb emission of PEG–PAA–Er at ~1 525 was dramatically enhanced by 250-fold. In addition, the PEG–PAA–Er/Yb complex can be used for the construction of molecular logic gates with AND logic functions and optical anticounterfeiting.

CRediT Author Statement

Yanling Yang: conceptualization, data curation, formal analysis, funding acquisition, investigation, methodology, project administration, writing original draft. **Fengyue Wang:** conceptualization, data curation, investigation, methodology, writing original draft. **Shan Zhang:** synthesis and characterization of PEG_{112}–PAA_{12}. **Hongxin Zhang and Zhen Yang**: conceptualization, data curation, formal analysis, investigation, project administration, writing review & editing.

Acknowledgements

This work was financially supported by the National Natural Science Foundation of China (Nos. 22104056, 62288102, and 82302356), Natural Science Foundation of Jiangsu Province (No. BK20210176), 2021 JiangSu Shuangchuang (Mass Innovation and Entrepreneurship) Talent Program (No. JSSCBS20210040), the Open Research Fund of State Key Laboratory of Digital Medical Engineering of Southeast University (No. 5507059002), the Natural Science Foundation of Fujian Province (No.

2023J01529), and the innovation team of photoelectric functional materials and devices for biomedical theranostics of Fujian Normal University (No. Y07204080K13).

Conflict of Interests

The authors have no conflicts of interest to declare.

Supporting Information

Supporting information to this article can be found online at https://doi.org/10.26599/NBE.2024.9290107.

References

[1] F.F. Wang, F.Q. Ren, Z.R. Ma, et al. *In vivo* non-invasive confocal fluorescence imaging beyond 1, 700 nm using superconducting nanowire single-photon detectors. *Nature Nanotechnology*, 2022, 17(6): 653–660. https://doi.org/10.1038/s41565-022-01130-3

[2] G.S. Hong, A.L. Antaris, H.J. Dai. Near-infrared fluorophores for biomedical imaging. *Nature Biomedical Engineering*, 2017, 1: 10. https://doi.org/10.1038/s41551-016-0010

[3] D.J. Naczynski, M.C. Tan, M. Zevon, et al. Rare-earth-doped biological composites as *in vivo* shortwave infrared reporters. *Nature Communications*, 2013, 4: 2199. https://doi.org/10.1038/ncomms3199

[4] Y.L. Yang, Y.L. Liu, J.H. Weng, et al. A carbonic anhydrase-targeted NIR-II fluorescent cisplatin theranostic nanoparticle for combined therapy of pancreatic tumors. *Biomaterials*, 2024, 305: 122454. https://doi.org/10.1016/j.biomaterials.2023.122454

[5] Z.H. Hu, C. Fang, B. Li, et al. First-in-human liver-tumour surgery guided by multispectral fluorescence imaging in the visible and near-infrared-I/II windows. *Nature Biomedical Engineering*, 2019, 4(3): 259–271. https://doi.org/10.1038/s41551-019-0494-0

[6] H. Wan, J.Y. Yue, S.J. Zhu, et al. A bright organic NIR-II nanofluorophore for three-dimensional imaging into biological tissues. *Nature Communications*, 2018, 9: 1171. https://doi.org/10.1038/s41467-018-03505-4

[7] E.D. Cosco, B.A. Arús, A.L. Spearman, et al. Bright chromenylium polymethine dyes enable fast, four-color *in vivo* imaging with shortwave infrared detection. *Journal of the American Chemical Society*, 2021, 143(18): 6836–6846. https://doi.org/10.1021/jacs.0c11599

[8] Y.L. Yang, S.F. Wang, L.F. Lu, et al. NIR-II chemiluminescence molecular sensor for In Vivo high-contrast inflammation imaging. *Angewandte Chemie International Edition*, 2020, 59(42): 18380–18385. https://doi.org/10.1002/anie.202007649

[9] V.G. Bandi, M.P. Luciano, M. Saccomano, et al. Targeted multicolor *in vivo* imaging over 1, 000 nm enabled by nonamethine cyanines. *Nature Methods*, 2022, 19(3): 353–358. https://doi.org/10.1038/s41592-022-01394-6

[10] S.Q. He, J. Song, J.L. Qu, et al. Crucial breakthrough of second near-infrared biological window fluorophores: Design and synthesis toward multimodal imaging and theranostics. *Chemical Society Reviews*, 2018, 47(12): 4258–4278. https://doi.org/10.1039/c8cs00234g

[11] H.X. Zhang, Y. Fan, P. Pei, et al. Tm^{3+}-sensitized NIR-II fluorescent nanocrystals for In Vivo information storage and decoding. *Angewandte Chemie International Edition*, 2019, 58(30): 10153–10157. https://doi.org/10.1002/anie.201903536

[12] H.B. Xu, Y. Yang, L.F. Lu, et al. Orthogonal multiplexed NIR-II imaging with excitation-selective lanthanide-based nanoparticles. *Analytical Chemistry*, 2022, 94(8): 3661–3668. https://doi.org/10.1021/acs.analchem.1c05253

[13] Z.R. Ma, M.X. Zhang, J.Y. Yue, et al. Near-infrared IIb fluorescence imaging of vascular regeneration with dynamic tissue perfusion measurement and high spatial resolution. *Advanced Functional Materials*, 2018, 28(36): 1803417. https://doi.org/10.1002/adfm.201803417

[14] H.C. Yang, H.Y. Huang, X. Ma, et al. Au-doped Ag_2Te quantum dots with bright NIR-IIb fluorescence for *in situ* monitoring of angiogenesis and arteriogenesis in a hindlimb ischemic model. *Advanced Materials*, 2021, 33(37): 2103953. https://doi.org/10.1002/adma.202103953

[15] B. Huang, T. Tang, S.H. Chen, et al. Near-infrared-IIb emitting single-atom catalyst for imaging-guided therapy of blood-brain barrier breakdown after traumatic brain injury. *Nature Communications*, 2023, 14: 197. https://doi.org/10.1038/s41467-023-35868-8

[16] P. Pei, Y. Chen, C.X. Sun, et al. X-ray-activated persistent luminescence nanomaterials for NIR-II imaging. *Nature Nanotechnology*, 2021, 16(9): 1011–1018. https://doi.org/10.1038/s41565-021-00922-3

[17] X.Y. Zhu, X. Liu, H.X. Zhang, et al. High-fidelity NIR-II multiplexed lifetime bioimaging with bright double interfaced lanthanide nanoparticles. *Angewandte Chemie International Edition*, 2021, 60(44): 23545–23551. https://doi.org/10.1002/anie.202108124

[18] T. Wang, S.F. Wang, Z.Y. Liu, et al. A hybrid erbium(III)–bacteriochlorin near-infrared probe for multiplexed biomedical imaging. *Nature Materials*, 2021, 20(11): 1571–1578. https://doi.org/10.1038/s41563-021-01063-7

[19] S.V. Eliseeva, J.C.G. Bünzli. Lanthanide luminescence for functional materials and bio-sciences. *Chemical Society Reviews*, 2010, 39(1): 189–227. https://doi.org/10.1039/b905604c

[20] C. Doffek, N. Alzakhem, C. Bischof, et al. Understanding the quenching effects of aromatic C–H- and C–D-oscillators in near-IR lanthanoid luminescence. *Journal of the American Chemical Society*, 2012, 134(39): 16413–16423. https://doi.org/10.1021/ja307339f

[21] A. Mech, A. Monguzzi, F. Meinardi, et al. Sensitized NIR erbium(III) emission in confined geometries: A new strategy for light emitters in telecom applications. *Journal of the American Chemical Society*, 2010, 132(13): 4574–4576. https://doi.org/10.1021/ja907927s

[22] G. Mancino, A.J. Ferguson, A. Beeby, et al. Dramatic increases in the lifetime of the Er^{3+} ion in a molecular complex using a perfluorinated imidodiphosphinate sensitizing ligand. *Journal of the American Chemical Society*, 2005, 127(2): 524–525. https://doi.org/10.1021/ja0441864

[23] C.Y. Chow, S.V. Eliseeva, E.R. Trivedi, et al. Ga^{3+}/Ln^{3+} metallacrowns: A promising family of highly luminescent lanthanide complexes that covers visible and near-infrared domains. *Journal of the American Chemical Society*, 2016, 138(15): 5100–5109. https://doi.org/10.1021/jacs.6b00984

[24] E.R. Trivedi, S.V. Eliseeva, J. Jankolovits, et al. Highly emitting near-infrared lanthanide "encapsulated sandwich" metallacrown complexes with excitation shifted toward lower energy. *Journal of the American Chemical Society*,

2014, 136(4): 1526−1534. https://doi.org/10.1021/ja4113337

[25] Z. Zhang, C. Zheng, Y. Wang, et al. Removal of hydroxyl groups to enhance the near- and mid-infrared emission of heavy-metal oxyfluoride glasses by chemical clarification: Nitrate ions. *Journal of Non-Crystalline Solids*, 2020, 544: 120165. https://doi.org/10.1016/j.jnoncrysol.2020.120165

[26] Y.T. Yang, S.Y. Zhang. Spectral study of the co-luminescence effect of lanthanide ternary complexes with benzoic acid and phenanthroline. *Spectroscopy Letters*, 2004, 37(1): 1−10. https://doi.org/10.1081/sl-120028419

[27] Z.Y. Li, R.J. Ma, Y.L. An, et al. Micellization and luminescence of PEG-b-P4VP/europium(III)/1, 10-phenanthroline complex. *Colloid and Polymer Science*, 2010, 288(9): 1041−1046. https://doi.org/10.1007/s00396-010-2237-3

[28] Y.W. Wang, S.B. Liu, Y.L. Yang, et al. A terbium(III)-complex-based on–off fluorescent chemosensor for phosphate anions in aqueous solution and its application in molecular logic gates. *ACS Applied Materials & Interfaces*, 2015, 7(7): 4415−4422. https://doi.org/10.1021/am5089346

[29] Z.T. Qin, H.E. Guo, X.Z. Cheng, et al. Recent advances of logic gate circuits based on metallo-organic compounds. *ACS Materials Letters*, **2024**, 6(4): 1504–1521. https://doi.org/10.1021/acsmaterialslett.4c00073

[30] Y.T. Guo Z.Y., Li, B.C. Guo, et al. Targeting-specific nanoprobes in the second near-infrared window for biomedical applications. *Nano Biomedicine and Engineering*, 2024, 16(2): 135−151. https://doi.org/10.26599/nbe.2024.9290061

[31] L. Liu, J.P. Shi, Y.A. Li, et al. Disguise as fluorescent powder: Ultraviolet-B persistent luminescence material without visible light for advanced information encryption and anti-counterfeiting applications. *Chemical Engineering Journal*, 2022, 430: 132884. https://doi.org/10.1016/j.cej.2021.132884

[32] B. Yan. Multiple luminescence responsive chemical sensing of lanthanide functionalized metal-organic frameworks hybrids for logic gate operation application to construct intelligent detecting platform. *TrAC Trends in Analytical Chemistry*, 2024, 170: 117430. https://doi.org/10.1016/j.trac.2023.117430

[33] C.Y. Zhang, Q.X. Yin, S.K. Ge, et al. Optical anti-counterfeiting and information storage based on rare-earth-doped luminescent materials. *Materials Research Bulletin*, 2024, 176: 112801. https://doi.org/10.1016/j.materresbull.2024.112801

[34] E. MacKenzie Lewis, P. Robert. Circularly polarized lanthanide luminescence for advanced security inks. *Nature Reviews Chemistry*, 2020, 5(2): 109−124. https://doi.org/10.1038/s41570-020-00235-4